Surgical Retraction of Non-Uniform Deformable Layers of Tissue:
2D Robot Grasping and Path Planning

Rik Jansen, 0366013

August 27, 2015

Abstract

This thesis considers robotic automation of a common *surgical retraction* primitive of exposing an underlying area by grasping and lifting a thin, 3D, possibly inhomogeneous layer of tissue. We present an algorithm that computes a set of stable and secure grasp-and-retract trajectories for a point-jaw gripper moving along a plane, and runs a 3D finite element (FEM) simulation to certify and assess the quality of each trajectory. To compute secure candidate grasp locations, we use a *continuous spring* model of thin, inhomogeneous deformable objects with linear energy potential. Experiments show that this models produces stress-metrics that strongly correlate with those resulting from an exhaustive optimization with an FEM mesh, but is orders of magnitude cheaper: our method runs in $O(v \log v)$ time, where v is the number of veins, while the FEM computation takes $O(pn^3)$ time, where n is the number of nodes in the FEM mesh and p is the number of nodes on its perimeter. Furthermore, we present a constant tissue curvature (CTC) retraction trajectory that distributes strain uniformly around the medial axis of the tissue. 3D FEM simulations show that the CTC achieves retractions with lower tissue strain than circular and linear trajectories. Overall, our algorithm computes and certifies a high-quality retraction in about one minute on a PC.

Contents

Chapter 1

Introduction

Robotic surgical assistants (RSAs) can enhance a surgeon's precision and dexterity in laparoscopic procedures, but are currently teleoperated directly as slave devices completely under the surgeon's control. Automation of commonplace surgical tasks could help surgeons focus attention on more critical components of surgery. It may also help surgeons perform complex procedures with three or more manipulators operated simultaneously. Furthermore, automation may enable RSAs to perform procedures in battlefields, where trained medical personnel are scarce, and in remote locations, where large time delays hamper direct teleoperation. This thesis describes initial steps toward automating *retraction* in robotic surgery, a common task where an outer covering of tissue is pulled away to expose an underlying area of interest (Fig. 1.1).
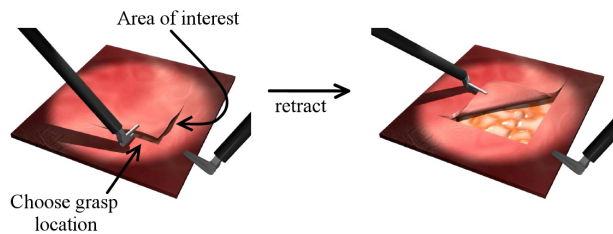
Figure 1.1: Automatically retracting a layer of tissue to expose an area of interest. The robot should place its gripper to minimize strain of the retraction.

We consider a restricted problem, illustrated in Fig. 1.2. The retraction takes place in 3D, but the 2-point-jaw gripper moves on a 2D plane, and the tissue is assumed to be a thin layer connected at one side. To expose the underlying area of interest with sufficient clearance for subsequent tasks, the gripper must pull the tissue above a line AB (a hard objective). It also should not impart large strains that may damage the tissue (a soft objective). Our problem allows the tissue to be heterogeneous, which we illustrate by embedding stiffer "veins" in the softer surrounding tissue.
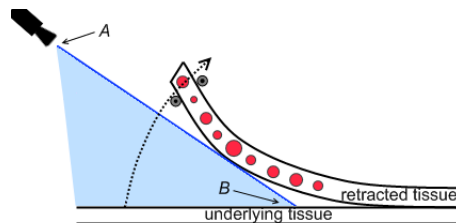
Figure 1.2: 2D tissue retraction problem. The RSA must expose a point of interest (point B) to the camera (point A) by moving the tissue to lie completely above AB .

Before executing a retraction on a real patient, we assume that the RSA must be issued a *certificate* from a trusted 3D finite element (FEM) simulator that states the clinical objectives are likely to be achieved (this simulator is assumed given, and outside the scope of this writing). The RSA must find and certify a retraction quickly to remain responsive in the changing surgical environment. We aim to reduce the number of queries to the computationally expensive FEM simulator. To do so, we use simplified models to help generate candidate retractions that are fast to compute, high-quality, and likely (but not guaranteed) to be certified.

These models decompose the 2D cross-section of tissue into a string of parallel 1D components, where the components are orthogonal to the medial axis. Crosswise, a *continuous spring model* is used to quickly determine a set of candidate grasp locations that make use of tissue heterogeneity to ensure locally *stable* grasp (using a method similar to the D-Space algorithm [7]). Lengthwise, the tissue is treated as a cantilever beam, and we derive an analytical solution for the *constant tissue curvature* (CTC) retraction trajectory for a given grasp location. Experiments show that stress-metrics computed by the continuous spring model correlates strongly with those computed by the original D-Space algorithm, but is faster by orders of magnitude. These stress-measures are used to find stable and secure grasps. We also show the CTC trajectory causes lower tissue strains than circular and linear trajectories. The combined algorithm can typically produce and certify high-quality retraction trajectories in about one minute on a PC.

Chapter 2

Related Work

2.1 Robotic surgical assistants

Several robots have been proposed for minimally invasive laparoscopic surgery, for example by Cavusoglu et. al. [4], Guthart and Salisbury [8], and Madhani et. al. [16]. Intuitive Surgical's daVinci^{TM} system has been commercialized and used in thousands of surgical procedures [8]. The surgeon uses a console with visual and tactile feedback to teleoperate a pair of manipulator arms that enter the body cavity. Several methods help improve the precision of such robots, including steady-hand systems [25] and motion scaling [8]. Nevertheless, these procedures remain under direct control of the surgeon. Some semi-supervised robots have been used in specific medical applications, such as neurosurgery [24], radiation therapy [26], and prostate brachytherapy [6].

2.2 Grasping deformable objects

A large body of work has addressed grasping and fixturing of rigid objects (see Bicchi and Kumar [2] for a survey), with some work extended to deformable objects. Cheong, et. al addressed fixturing problems for an articulated chain of polygons [5]. Cai et. al. and Menassa et. al. investigated deformable sheet-metal parts while minimizing part deformation [3, 18]. Howard and Bekey used a learning approach to enable grasping of deformable objects using tactile feedback [12]. Yu et. al. studied the behavior of controllers for grasping soft tissue [28].

The notion of D-Space was introduced by Gopalakrishnan and Goldberg [7] to characterize the security of grasped deformable parts modeled by a FEM mesh. A configuration in D-Space is represented by all DOFs of the nodes of the mesh, and stable configurations require positive work to release the object from its grasp. An algorithm for finding an optimal jaw separation distance was also introduced for a two-point gripper that balances the energy needed to release the part against the energy needed to compress it into plastic deformation [7]. We use a simplified version of this technique to select secure grasps of a thin tissue layer.

2.3 Manipulating deformable objects

A number of researchers have addressed motion planning for deformable linear objects such as ropes and cables. Saha et. al. describe a sampling-based motion planner for rope manipulation with two cooperating robot arms [23]. Moll and Kavraki describe a method for computing energy-minimizing curves subject to manipulation constraints, and apply them to surgical suturing problems [20]. Holleman et. al. and Lamiraux and Kavraki developed path planners for elastic surface patches [11,

14]. The surface patch is modeled as a Bezier surface with low bending energy, and a sampling-based planner is used to plan the path.

Other work has addressed planning for volumetric deformations. Rodriguez et. al. applied sample-based planning to deformable objects in deformable 3D environments [22]. Alterovitz et. al. used a numerical optimization approach to plan needle paths in 2D deformable tissue for prostate brachytherapy [1]. Hirai et. al. [10] presented the use of visual feedback to position points in 2D deformable tissue, which was applied in breast biopsies [17] and prostate brachytherapy [27].

Chapter 3

Background

This section provides a textuel description of concepts used in this thesis. For a rigorous mathematical explanation, see [15].

3.1 Elasticity Theory

In Solid Mechanics, a deformable *body* is considered as a bounded region of material points (a *continuum*) having a given *density* (i.e. mass per unit area). In a continuum, all quantities (e.g. density or displacement) are assumed to vary continuously. A body with constant density is called *homogeneous*. A body with varying density is called *heterogeneous*. The initial configuration of a body is defined as the configuration that has no external forces acting upon it.

3.1.1 Strain

When forces are applied to the continuum, the absolute changes in position of the material points over time is described by a *displacement field*. If the displacement field is constant, a rigid-body displacement occurs. In contrast, a deformation displacement takes place when relative displacements occur between material points, as measured by the spatial gradient in the displacement field. Notice that the spatial gradient at a material point is orientation dependent (i.e. deformation can independently happen along any dimension). It is measured by the *strain*-tensor; a tensor is a linear function that maps between vector quantities (in this case, from the direction vector to strain).

Intuitively, strain describes the change of shape of an infinitesimal cube, which can be further decomposed into a stretch-component and a rotational component. In the case of pure stretch, strain represents the ratio of deformation-length to initial length.

3.1.2 Stress

As a material deforms, internal forces will try to restore the body to its initial, non-deformed shape. In order to be in static equilibrium, the net force at any material point must be zero. This entails that any cross-sectional separating plane through the body must be in static equilibrium, meaning that the force per unit area exerted by the side in the direction of the normal to the separation-plane (called the *traction*) must be exactly counter-acted by forces exerted by the opposite side of the plane (regardless of its complex composition). The part of the traction that is normal to the separating plane is called *normal stress*, while the in-plane part is called *shear stress*. As is apparent, at any material point, the traction depends on the direction of the separating plane through the material

point. Therefore, the internal forces are described by the *stress*-tensor (mapping the normal vector to the traction vector).

For any stress-tensor, it is always possible to find an orientation for the normal of the separating surface, such that the shear-stresses will vanish. In this configuration, only the normal shear contributes to the traction, and is called the *principal stress*.

3.1.3 The linear Stress-Strain Relationship

Stress and strain are coupled in elastic media by a stress-strain or *constitutive* relationship, which is completely dependent on the specific material at hand. If we assume the material is linearly elastic (which is a good approximation for small deformations), the relationship is described by a so-called *fourth-order* tensor (as it relates a strain-tensor to a stress-tensor) and requires 21 independent components. If, however, the behavior of the material is equal in any direction, we call it *isotropic* and the constitutive law depends on only 2 material properties: *Young's modulus* and *Poisson's ratio*. Young's modulus measures the force per unit area needed to stretch a material one unit distance. Poisson's ratio measures how compression in one direction effects compression in the other directions. Both these properties are experimentally observed.

The constitutive relationship only holds in the *elastic region* of the material, which is the range of strains the material can fully recover from when external forces are removed. It is therefore important to regard the *elastic limit*, which denotes the upper bound of this region.

3.1.4 Ideal Linear Springs

When the deformable body is restricted to a one-dimensional object, the body is called a *linear spring*. The constitutive law in this scenario is known as *Hooke's Law*, that states the resulting force due to compression is proportional to the compressed distance σ of the spring (within the elastic range). The constant of proportionality k is called the *spring constant* and is analogous to the Young's modulus.

A spring can be seen as a device that stores *elastic potential energy*. The amount of energy E stored is given by

$$E = \frac{1}{2}k\sigma^2$$

Springs are particularly elegant in the way they can combine into new physical systems. In particular, when a spring with spring constant k_1 is serially connected to a spring with spring constant k_2, we can regard the combined spring as a single spring with *equivalent spring constant* $k_{eq} = k_1 + k_2$.

3.2 Finite Element Methods (FEM)

The stress-strain and strain-displacement relationships as described in the previous subsection ultimately lead to a set of *partial differential equations (PDEs)*, equations relating multi-variable functions and their partial derivatives, which must hold over the continuum. In order to solve these equations (whose solutions are functions), *initial conditions*, describing the initial state of the system (e.g. external forces) as well as *boundary conditions*, describing restrictions at the boundary of the continuum, must be specified.

Analytical methods exist to solve simple (in terms of domain) PDEs. In general, however, numerical methods must be used to solve these systems. One family of such methods is called *Finite Element Methods (FEMs)*. FEMs discretize the continuum into a finite set of *elements*

(having simple shapes), which meet each other at *nodes*. The topology of these elements are captured by a *mesh*. This reduces the problem of solving over a complex domain to solving only for a finite number of elements with simple domains on which we assume the solutions have a simple form. Of course, the elements are connected through shared nodes, so all elements must be solved for simultaneously. Several methods exists to translate the governing PDEs of the system to linear systems for the elements [19]. Once these systems are derived, they are gathered in one large (and often sparse) *Stiffness Matrix*. Together with the initial conditions (which are described by a vector), a linear equation results, which can be solved by any numerical solver.

Chapter 4

Problem Statement

4.1 Tissue and Robot Modeling

We model the tissue as a 3D elastic deformable body E, which we assume is a thin layer of uniform thickness having known material properties. For simulation purposes, E is represented into a tetrahedral FEM mesh. Heterogeneous tissue is modeled by a mesh with varying stiffness. The D-Space of all 3D FEM mesh configurations is denoted by D, and $q \in D$ describes all positions of the simulation nodes. We forward simulate FEM dynamics using the method of Irving et. al. [13]. Our retraction algorithms assume that the tissue is damped and velocities of the jaws remain low, such that the tissue moves smoothly between time steps and its motion can be approximated as a quasi-static process.

The gripper is modeled by two point contacts moving on a planar cross section of 3D space. We take a frame of reference such that the bottom edge of the tissue cross section lies on the x axis, and gravity acts in the $-y$ direction. The 4D space of robot configurations is denoted C.

4.2 Retraction Trajectories

A retraction is a robot trajectory $c(t) : [0, T] \mapsto C$, for some unknown termination time T. We do not consider how the robot moves before it makes initial contact, so that the jaws are instantaneously placed at points on the perimeter of the tissue at time $t = 0$. First, the jaws are compressed, and then the gripper is moved while keeping the distance between jaws fixed. At time $t > 0$, the motion of the tissue in response to $c(t)$ can be computed by evaluating the FEM simulation. Let this path be denoted $q_c(t) : [0, T] \mapsto D$.

4.3 Visibility, Grasp Security, and Strain Objectives

Our problem is to produce a retraction $c(t)$ and a termination time T that meets the following objectives.

1. *Visibility.* Given view point A and a point B on the area of interest, we require that at time T the tissue at configuration $q_c(T)$ lies above line AB.

2. *Grasp security.* Grasp points must stay fixed relative to the tissue throughout the retraction (i.e. do not break contact or slip). We assume the friction coefficient μ between the gripper and tissue is known.

3. *Admissible strain.* To cope with noise and discretization artifacts in the FEM mesh, we require that the average strain $\epsilon_{max}(c)$ of the 1% volume elements with the highest strain does not exceed the strain limit ϵ_L.

The FEM simulation issues a certificate to retraction $c(t)$ if these objectives are satisfied after $c(t)$ is simulated. We assume that the simulation is trusted by the surgeon, so that a certified retraction is safe to execute on the patient. We consider strain as a soft objective function, so given multiple certified trajectories we select the retraction with lowest $\epsilon_{max}(c)$.

Chapter 5

Method

Our approach generates a number of candidate retractions (up to a user-defined maximum), and tests the objectives of chapter 4.3 by evaluating the FEM simulation. To generate the retractions, we first pick a set of contact pairs p_a and p_b which are likely to be locally stable, using a simplified linear spring model. For each contact pair p_a and p_b, we first close the jaws to a distance that trades off stability against tissue strain. Then, holding the distance constant, we move the gripper along a trajectory that is optimal if the tissue layer is viewed as a homogeneous cantilever beam under no gravity.

5.1   Choosing stable grasp locations

We choose grasp locations that are locally optimal with respect to the grasp security and admissible strain objectives, while we consider the visibility constraint at a later stage. Gopalakrishnan and Goldberg [7] define *stable* grasps as pairs of perimeter nodes that are located at local minima in the elastic potential of the FEM mesh, and they describe an algorithm that finds a jaw distance that trades off stability against plastic deformation. Finding the optimal distance for a n-nodes mesh with p perimeter nodes takes $O(n^3 p^2 + p^6 \log p)$ time. Our approach uses the same concepts, but introduces simplifications appropriate for a thin rectangular mesh.

5.1.1   Stable grasps and escape energy

Our tissue is considered a thin layer of uniform thickness, where *thickness* ϕ measures the ratio between the gripper compression distance σ and the initial distance d between the grippers at the perimeter of the layer.

$$\phi = \frac{\sigma}{d} \qquad , \sigma < d$$

Using the assumption of uniform thickness, we can simplify the solutions as described by Gopalakrishnan and Goldberg [7]. In their framework, jaws are assumed frictionless and the jaws are contracted towards each other. We shall follow these conventions here and note that in order to improve stability, we require that the jaws must be directly opposite the mesh surface, as illustrated in Fig. 5.1. This additional requirement fixes d to our tissue height h and also reduces our problem to finding an optimal horizontal translation x along the length of the tissue. Consider tissue stiffness as a function of x. We let $k_{eq}(x)$ denote the *equivalent spring constant*, which represents the amount of force at x needed to compress the tissue a unit distance. We characterize the stability of a grasp location x by its ability to resist shifting to a neighboring spring. That is, a grasp at x
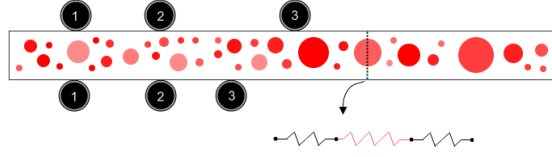
Figure 5.1: A continuous model for representing heterogeneous tissue. Darker shaded areas represent veins. Jaws as shown in positions 1 and 2 are allowed. Asymmetric grasps, such as position 3, are not allowed. The line segment running from the upper surface to the lower surface between the jaws is considered as a serial connected spring with varying spring constants.

is *stable* if positive work is needed to shift the grasp from x to x'. This is precisely the case where x corresponds to a local minimum of $k_{eq}(x)$.

Escaping the basin of attraction of a stable grasp requires sliding the grasp past a local maximum of $k_{eq}(x)$. We use the following *escape potential* metric to characterize the stability of a stable grasp location x:

$$Escape(x) = \min(k_{eq}(x_r), k_{eq}(x_l)) - k_{eq}(x) \tag{5.1}$$

where x_r and x_l are respectively the local maxima to the right and left of x. Thus, to find all stable grasp locations and calculate their escape potential, we must simply find the extreme points of k_{eq}.

5.1.2 Locally stable grasp locations using a continuous spring model

Though, in principle, it would be possible to compute k_{eq} using the FEM model, we use a much faster *continuous spring model* approximation, which uses our uniform thickness assumption. In order to do so, we first turn our attention to the field of *Contact Mechanics*.

Consider a half-plane having normal $\mathbf{e_2}$ with a tangential force F_1 and normal force F_2 applied at the origin (Fig. 5.2). Under the conditions of *plane stress*, it is shown by Flamant [4] that
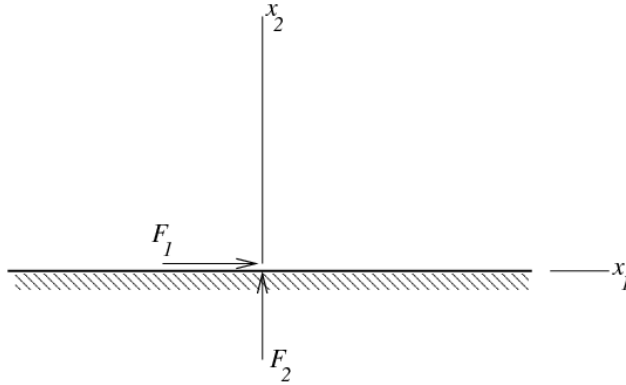
Figure 5.2: Forces F_1 and F_2 applied to a half-plane.

the distribution of increase in stresses resulting from the applied forces are as follows (in polar coordinates):

$$\sigma_r = \frac{-2}{\pi\,r}(F_1\,\cos\theta + F_2\,\sin\theta) \tag{5.2}$$

$$\sigma_{r\theta} = 0 \tag{5.3}$$

$$\sigma_\theta = 0 \tag{5.4}$$

As is apparent from these formulae, the only varying stress-component is σ_r, which varies as $\frac{1}{r}$ and takes its maximal values along $\theta = -\arctan\left(\frac{F_1}{F_2}\right)$ for fixed r. We shall call the line through the origin with this direction the *line-of-maximal-stress*. In particular, when $[\mathbf{F_1}\mathbf{F_2}] = -\mathbf{e_2}$ (i.e. the point-load acts normal into the half-space, as is the case for our grippers), the *line-of-maximal-stress* equals $\theta = -\frac{\pi}{2}$.

Returning our attention to our thin layer of uniform height, we can, geometrically speaking, regard our layer to be the intersection of two half-spaces. Applying the Flamant solution to our situation, we are violating the assumption of an unbounded half-space. We shall assume, however, that when we transition from the unbounded half-space to the finite width layer, the lines-of-maximal-stress for each individual gripper will remain the same. To support our assumption, fig. 5.3 shows the stress distribution as computed by ANSYS for grippers acting normally into the layer.
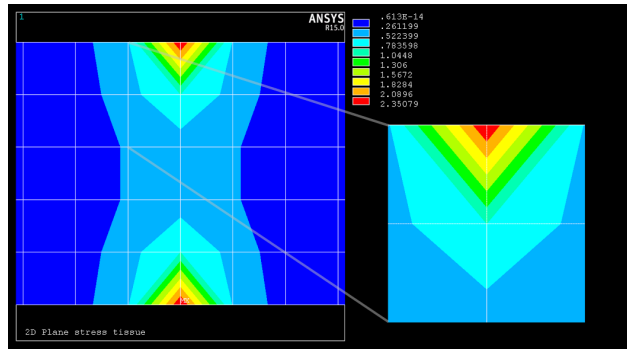
Figure 5.3: FEM simulation showing maximal stress occurs on the line-of-maximal-stress.

Using our findings of maximal stress occurring on the *line-of-maximal-stress*, we approximate the tissue's compression behavior as a vertical linear spring along a slice through the tissue (Fig. 5.1). This approximation decouples each slice from its neighboring tissue, and therefore ignores interactions due to shear stress. If the tissue is sufficiently thin, shear stresses will not affect the compression behavior much.

Consider the line segment $s_{cross}(x)$ running vertically through the tissue between the jaws placed at x. We can decompose it into multiple line segments s_i with length $l_i(x)$, each of which has constant Young's moduli E_i and infinitesimal cross section A. Each segment s_i can be considered as a spring with spring constant $k_i(x) = \frac{E_i}{l_i(x)}$. The combined serial spring $s_{cross}(x)$ has an equivalent spring constant $k_{eq}(x)$:

$$k_{eq}(x) = \frac{1}{\sum_{i=1}^{n} \frac{1}{k_i(x)}} = \frac{1}{\sum_{i=1}^{n} \frac{l_i(x)}{E_i}}. \tag{5.5}$$

If veins are represented as polygons with v vertices, we can compute the extreme points of k_{eq} using a sweep line algorithm. We note that the extreme points of $k_{eq}(x)$ are also extreme points of $\frac{1}{k_{eq}(x)}$, and $\frac{1}{k_{eq}(x)}$ is a sum of linear functions. Considering vertices as event points, we find when $1/k_{eq}(x)$ changes slope for each vertex encountered in the event queue. Sorting the queue takes $O(v \log v)$ time, and each of the v event points can be evaluated in $O(1)$ time, which leads to an $O(v \log v)$ running time overall.

Fig. 6.1 shows an example of the equivalent spring constant function constructed by the sweep-line method using a fine polygonalization of the veins.

5.2 Choosing an optimal jaw distance

Once we have chosen a location to grasp the tissue, we must choose a compression distance σ. We use a criterion similar to the one used in Gopalakrishnan and Goldberg [7] that balances the competing objectives of grasp security and low strain, in particular, we choose σ such that the energy needed to release the grasp is equal to the energy needed to exceed the strain limit. Consequently, jaw compression can be reduced when the tissue is heterogeneous and the grasp location is locally secure (i.e., bordered by relatively stiff veins). In turn, this reduces tissue strain.

We choose σ as follows. Let the tissue at the grasp point have the equivalent spring constant K_{eq}. Closing the jaws to distance σ induces strain $\epsilon = 1 - \sigma/L$ where L is the rest height of the tissue. The elastic strain limit ϵ_L imposes the constraint $\sigma \geq (1 - \epsilon_L)L$. Given σ, the amount of energy needed to compress the spring to the strain limit is

$$U_L(\sigma) = \frac{1}{2}K_{eq}(\sigma - (1 - \epsilon_L)L)^2 \tag{5.6}$$

We also find the smallest of both nearest maxima of the the function k_{eq} around the grasp point and let K_n denote its equivalent spring constant. If the tissue is locally homogeneous, we set $K_n = K_{eq}$. The amount of energy U_n to compress the neighboring spring a distance σ equals:

$$U_n(\sigma) = \frac{1}{2}K_n\sigma^2 \tag{5.7}$$

We choose σ such that (5.6) and (5.7) are equal:

$$\sigma = \frac{\sqrt{K_{eq}}(1 - \epsilon_L)L}{\sqrt{K_{eq}} + \sqrt{K_n}} \tag{5.8}$$

5.3 Choosing a Retraction Trajectory

After finding grasp locations p_a, p_b and a jaw separation distance σ, we must find a path of the manipulator to retract the tissue. Some simple paths (e.g. straight lines and circular arcs) can achieve the retraction objectives without causing excessively high strains, because the largest strains are usually caused by the squeezing of the gripper. But, they do stretch the tissue unnecessarily. Therefore, we introduce a *constant tissue curvature* (CTC) trajectory that keeps the medial axis of the tissue stretch-free and bend with a constant curvature. This trajectory produces minimal strain if the tissue is treated as a weightless homogeneous cantilever beam that can bend and stretch, where stretching strain is much higher than bending strain. This latter assumption implies that the length of the tissue should be kept constant. With length held constant, theories on beams prescribe that curvature should be uniform to minimize the maximum bending strain.

Place a coordinate frame with its origin at the lower-right corner of the tissue. Let $-L$ denote the position of the grasp point. Along $c(t)$, the lower edge of the tissue must describe a circular arc with constant length L but time-varying radius $R(t)$ and center $(0, R(t))$, as illustrated in Fig. 5.4. At $t = 0$, we have $R(t) = \infty$ and as t increases, $R(t)$ decreases, moving the center of the circle along the y-axis toward the x-axis. At the end time $t = T$, the arc must lie to the right of the line-of-sight.

We compute the goal radius $R_g = R(T)$ to be tangent to the line-of-sight. With a bit of algebra, this can be shown to be:

$$R_g = \frac{|A - B||b_x a_y - a_x b_y| - (a_x - b_x)(a_x b_y - b_x a_y)}{(a_y - b_y)^2} \tag{5.9}$$
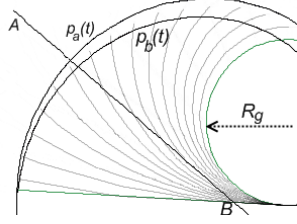
Figure 5.4: The trajectories $p_a(t)$ and $p_b(t)$ the jaw nodes follow during the retraction. The CTC path keeps the medial axis of the tissue circular with radius $R(t)$, length x, and, in the final configuration, lies tangent to the line-of-sight AB.

where $A = (a_x, a_y)$ and $B = (b_x, b_y)$. Intermediate tissue radii $R(t)$ are linearly interpolated in curvature as $R(t) = R_g \frac{T}{t}$.

At the tissue configuration at time t, the medial axis of the tissue will coincide with an arc of the circle with center $(0, R(t))$, but with radius $R(t) - \frac{1}{2}h$. Sliding along this arc with arc-length L, we compute the point $p(t)$:

$$
\begin{aligned}
p(t) &= ((R(t) - \tfrac{1}{2}h)\cos\theta, (R(t) - \tfrac{1}{2}h)\sin\theta + R(t)) \\
\theta(t) &= \frac{L}{R(t) - \frac{1}{2}h} + \tfrac{3}{2}\pi
\end{aligned}
$$

where the angle of the gripper θ is chosen to keep the arc-length fixed. At $c(t)$, the projections of the jaw locations on the medial axis should coincide with $p(t)$. Incorporating the jaw separations σ, the final CTC trajectory is:

$$
\begin{aligned}
p_a(t) &= (R_a(t)\cos\theta(t), R_a(t)\sin\theta(t) + R_a(t)) \\
p_b(t) &= (R_b(t)\cos\theta(t), R_b(t)\sin\theta(t) + R_a(t)) \\
R_a(t) &= R(t) - \sigma \\
R_b(t) &= R(t) + \sigma - h
\end{aligned}
$$

where p_a and p_b denote the location of the lower and upper jaw respectively. An illustration of such a path is given in Fig. 5.4.

To ensure the tissue is pulled past the line-of-sight in the presence of gravity and inhomogeneity, we generate a retraction trajectory that goes much longer than T, and let the FEM simulation run only until all objectives are met, or some constraint is violated.

Chapter 6

Experiments

All results in this chapter were obtained on a tissue model having dimension of 5.0 cm in length and 0.44 cm in height and depth, and density of $1\,\mathrm{g/cm^3}$. For 3D simulation we use Young Modulus and Poisson Ratio of 40 kPa and 0.45 respectively for the tissue and 200 kPa and 0.45 respectively for the vein. We set $\epsilon_L = 0.5$, and $\mu = 0.5$ throughout all experiments. The gravity for the dynamic simulation is set to $9.8\,\mathrm{m/s^2}$ downward. All experiments were performed on a PC with a 1.8 GHz processor and 2 GB of RAM.

6.1   Assessment of Grasp Selection Quality

We have compared our continuous spring method of computing stress with brute-force simulations with the commercial FEM package ANSYS. The FEM mesh contains ∼10,000 nodes and 160 pairs of opposite perimeter nodes. The diameters of the veins vary randomly in diameter between 10% and 60% of the tissue thickness. The stiffness of the veins vary randomly between 100 and 1000 kPa.

In ANSYS, we enumerated each pair of opposite perimeter nodes, contracted the jaws and solved for the maximum strain in the tissue. The ANSYS simulation took ∼16 minutes on a single run, while the spring method took 0.1 seconds. In order to determine the degree of agreement between the two different methods, we compute the *Pearson product-moment correlation coefficient* r between their solutions, which is invariant to scaling and translation. The results for varying thickness of the tissue ϕ and density of veins ρ are summarized in Table 6.1.

Table 6.1: Agreement between the Continuous spring method and FEM simulation.

ϕ \ ρ	.2	.4	.6	.8
.25	+.80	+.72	+.66	+.59
.50	+.80	+.72	+.66	+.59
.75	+.80	+.72	+.66	+.59

The first thing to notice from these results is that the degree of agreement is invariant to tissue-thickness ϕ. This is not surprising, as all physical models we used are linear. Secondly, in interpreting these results ([9]) we conclude both methods correlate (very) strongly, but less as the density of veins increase, which can be explained as follows: As our model only accounts for stresses occuring on the line-of-maximal-stress, veins closely neigboring this line (but not actually on the line) are not accounted for. As the density of veins in the tissue increases, so does the probability of encountering such off-line veins, resulting in larger discrepancies between our model and the FEM model.

Fig. 6.1 shows a comparison between the equivalent spring constant function k_{eq} and stress-values as computed by brute-force FEM simulations using ANSYS. Our stability criterium for grasps is characterized by the extreme points of this function. As becomes clear from the comparison, our method produces extrema at approximately the same locations (and of approximately the same order) as the FEM method. A quantitative comparison where we order the grasps by our stability-criterium as given by Eq. 5.1 shows both models show high agreement on optimal grasps.
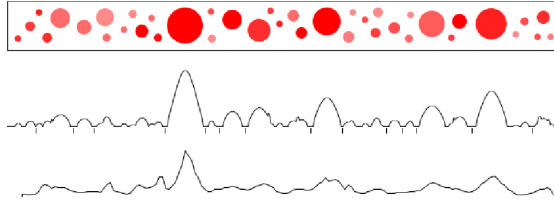
Figure 6.1: Top: tissue model. Vein opacity indicates stiffness. Middle and bottom: equivalent spring constants and stable grasp locations obtained by the continuous spring method (middle) and brute-force FEM simulations (bottom).

6.2 Assessment of Retraction Path Strains

In the following experiments, we use our 3D FEM simulator to compare the quality of our retraction trajectories (as described in Sec. 5.3) against linear and circular paths, which are attractive for their relative simplicity. For varying grasp location, we run linear paths with (1) 60° and (2) 75° slopes, (3) a circular path and (4) the CTC trajectory. In the linear and circular paths, we adjust the jaw orientations such that they are perpendicular to the line from the fixed end to the jaw's midpoint.

6.2.1 Experiments on homogeneous tissue

Fig. 6.2 plots the maximum strain during the simulation on homogeneous tissue with gravity for two lines-of-sight for 10 uniformly sampled grasping locations. We can see that the CTC path performs better than the circular and linear paths in all cases, even for suboptimal grasp locations.
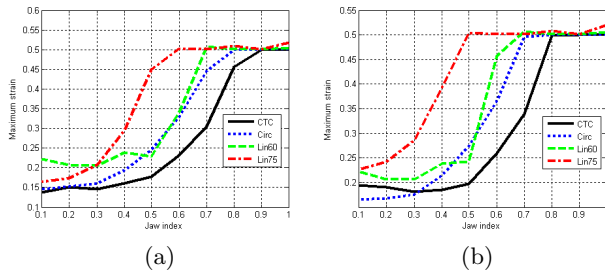
Figure 6.2: Comparing linear, circular and the CTC trajectories for two lines-of-sight, starting at distance (a) 25% and (b) 15% from the fixed end of the tissue. Each line-of-sight has 45° slope. Strain of 0.5 means failure.

Repeating the same experiment for other lines-of-sight, we found that the CTC trajectory almost always outperforms the other paths, except when the line-of-sight lies close to the fixed end of the tissue (approximately 25% away from the fixed end). In these cases, circular trajectories perform slightly better for certain grasp locations near the free end of the tissue.

In another set of experiments in homogeneous tissue we found that the optimal jaw location is relatively insensitive to problem parameters (e.g., line-of-sight, tissue thickness, and friction), and
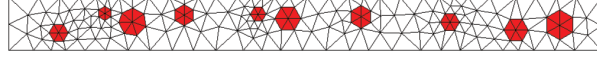
Figure 6.3: Side view of 3D FEM mesh containing 10 veins.
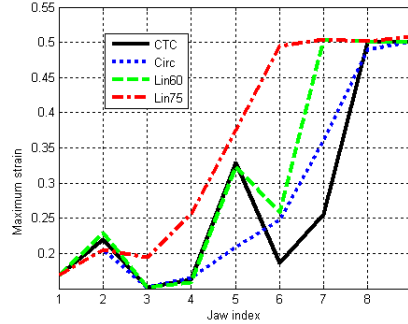
Figure 6.4: Comparing linear, circular, and constant-tissue-curvature (CTC) paths for heterogeneous tissue containing 10 veins. An index of i means the jaw is in a stable location between the i-th and $(i + 1)$-th vein.

nearly always lies between 10% and 20% from the free end of the tissue.

6.2.2 Experiments on heterogeneous tissue

In this chapter, we consider a heterogeneous tissue containing 10 veins (Fig. 6.3). For all candidate grasp locations found by the continuous spring method, we ran the 3D simulation using the linear, circular and CTC paths. Results are shown in Fig. 6.4. Both the CTC and the circular path are able to find the optimal jaw location between veins 3 and 4.

For suboptimal jaw locations, the CTC path usually outperforms other paths, except the circular path performs substantially better at jaw location 5. (Even under further scrutiny, we are unable to discern a clear cause for this behavior.) Apart from these occasional anomalies, this and other experiments suggests that the CTC trajectory still works well with heterogeneous tissue, even if a homogeneity assumption was used in its derivation.

6.3 Efficient Certification of Multiple Retractions

Given the multiple retractions computed by the continuous spring model, we wish to certify and choose the retraction that minimizes the maximum strain $\epsilon_{max}(c)$. Rather than run the FEM simulation in full for each retraction, we terminate simulations immediately when the hard objectives of Sec. 4.3 fail, or $\epsilon_{max}(c)$ exceeds the maximum strain computed for any prior certified retraction (because then c is suboptimal).

Our experiments in the heterogeneous tissue of Fig. 6.3 suggest that this pruning technique reduces running time from 286s to 76s for 10 veins. On a more complex mesh with 20 veins, pruning reduces running time from 819s to 95s. In most cases, the simulation trials were pruned early on, as strain is accumulated quickly during the compression phase and at the beginning of retraction.

6.4 Optimal Retraction for a Wide Piece of Tissue

Fig. 6.5 shows a screenshot from a retraction computed by our algorithm on a 3.5 cm wide heterogeneous tissue. The full animation accompanies this thesis as a supplemental video.
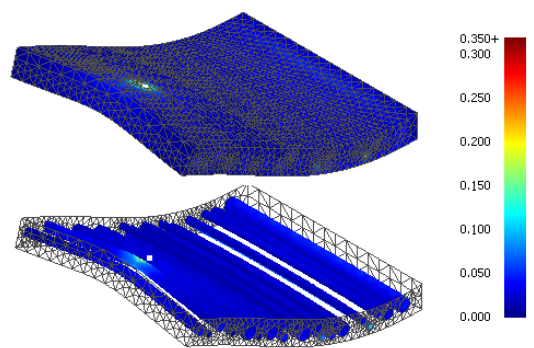
Figure 6.5: A frame from a 3D simulation of a 5 cm x 3.5 cm x 0.44 cm heterogeneous mesh with 20 veins, showing the surface of the mesh (top) and the veins (bottom). Strain is color coded.

Chapter 7

Conclusion and Future Work

This paper introduced a method to compute a trajectory for a two-point gripper, moving in a plane, to retract a thin layer of tissue under visibility and tissue strain constraints. We present a continuous spring model for finding locally stable candidate grasps in $O(v \log v)$ time, where v is the number of veins embedded in the tissue. For each candidate grasp location, we compute a retraction trajectory that causes a cantilever beam model of the tissue to follow a constant curvature arc. These retractions are then certified using a 3D finite element simulator. Experiments suggest that 1) the continuous spring approximation quickly computes many of the same grasp locations as an expensive FEM-based computation, and 2) constant-tissue-curvature paths produce lower tissue strains than circular or linear paths. Our algorithm can certify and select a high-quality retraction in about one minute on a PC.

In future work we hope to address more realistic manipulator models with geometric and kinematic constraints. One approach for incorporating complex grippers is computing the convolution between the equivalent-spring-constant-function and the gripper's profile-function. Only the part of the gripper compressing the tissue should be accounted for, so the gripper's profile-function would depend on the grasp distance into the tissue. Removing the constraint on the grippers to contract towards each other is also an interesting area of research. Allowing for this extra degree of freedom, the lines-of-maximal-stress for both grippers would not necessarily coincide, potentially resulting in less maximum stress. At the same time, depending on the spatial layout of the veins, more secure grasps could be achieved. Avoiding obstacles should also be addressed. In such a setting, regrasping may be necessary because of the limited accessibility of grasp points and limited range of motion of the tissue. More realistic tissue damage models would measure cellular damage as a function of strain and duration of applied load. Our method also does not perform the sophisticated spatial reasoning needed to find optimal retractions of thick tissue and retractions where tissue must be pulled apart rather than lifted. Similar reasoning would be necessary to optimize incision patterns and retractions simultaneously.

Since the publication of this work, follow-up work has been performed by Patil et. al. [21]. In their research, they consider a gripper with 6 DOFs manipulating a 3D flap of tissue. A sampling-based planner is used to compute trajectories between equilibrium configurations (as computed by a nonlinear FEM simulator), in order to generate a path between user-specified points in space. The paths are optimized to either minimize the maximum deformation energy, minimize maximum stress, or minimize the control effort. They successfully demonstrate that different optimization criteria yield different trajectories in two scenarios (including obstacle avoidance and heterogeneous tissues).

Acknowledgments

Bibliography

[1] R. Alterovitz, K. Goldberg, J. Pouliot, R. Taschereau, and I.-C. Hsu. Sensorless planning for medical needle insertion procedures. In *IEEE/RSJ Int. Conf. Int. Rob. and Sys.*, volume 4, pages 3337–3343, Oct. 2003.

[2] A. Bicchi and V. Kumar. Robotic grasping and contact: a review. In *IEEE/RSJ Int. Conf. Int. Rob. and Sys.*, pages 348–353, 2000.

[3] W. Cai, S. J. Hu, and J. X. Yuan. Deformable sheet metal fixturing : Principles, algorithms, and simulations. *J. of Manufacturing Science and Engineering*, 118(3):318–324, 1996.

[4] M. Cavusoglu, F. Tendick, M. Cohn, and S. Sastry. A laparoscopic telesurgical workstation. *IEEE Trans. Rob. and Aut.*, 15(4):728–739, Aug 1999.

[5] J.-S. Cheong, K. Goldberg, M. Overmars, and A. van der Stappen. Fixturing hinged polygons. In *IEEE Int. Conf. Rob. and Aut.*, pages 876–881, 2002.

[6] G. Fichtinger, E. C. Burdette, A. Tanacs, A. Patriciu, D. Mazilu, L. L. Whitcomb, and D. Stoianovici. Robotically assisted prostate brachytherapy with transrectal ultrasound guidance–phantom experiments. *Brachytherapy*, 5(1):14–26, Jan. 2006.

[7] K. G. Gopalakrishnan and K. Goldberg. D-space and deform closure grasps of deformable parts. *Int. J. of Rob. Res.*, 24(11):899–910, 2005.

[8] G. Guthart and J. Salisbury, J.K. The intuitive^TM telesurgery system: overview and application. In *IEEE Int. Conf. Rob. and Aut.*, pages 618–621 vol.1, 2000.

[9] D. Hinkle, W. Wiersma, and S. Jurs. *Applied statistics for the behavioral sciences*. Rand McNally College Pub. Co., 1979.

[10] S. Hirai, T. Tsuboi, and T. Wada. Robust grasping manipulation of deformable objects. In *IEEE Int. Symp. Assembly and Task Planning*, May 2001.

[11] C. Holleman, L. Kavraki, and J. Warren. Planning paths for a flexible surface patch. In *IEEE Int. Conf. Rob. and Aut.*, volume 1, pages 21–26, May 1998.

[12] A. M. Howard and G. A. Bekey. Recursive learning for deformable object manipulation. In *Proceedings of the 8th Int. Conf. on Advanced Robotics*, pages 939–944, 1997.

[13] G. Irving, J. Teran, and R. Fedkiw. Invertible finite elements for robust simulation of large deformation. In *Symp. on Computer Animation*, pages 131–140, 2004.

[14] F. Lamiraux and L. E. Kavraki. Path planning for elastic plates under manipulation constraints. In *IEEE Int. Conf. Rob. and Aut.*, pages 151–156, 1999.

[15] A. Love. *A Treatise on the Mathematical Theory of Elasticity*. Number v. 1 in A Treatise on the Mathematical Theory of Elasticity. Cambridge University Press, 2013.

[16] A. Madhani, G. Niemeyer, and J. Salisbury, J.K. The black falcon: a teleoperated surgical instrument for minimally invasive surgery. In *IEEE/RSJ Int. Conf. Int. Rob. and Sys.*, volume 2, pages 936–944, Oct 1998.

[17] V. Mallapragada, N. Sarkar, and T. Podder. Robot assisted real-time tumor manipulation for breast biopsy. In *IEEE Int. Conf. Rob. and Aut.*, 2008.

[18] R. Menassa and W. D. Vries. Optimization methods applied to selecting support positions in fixture design. *ASME J. of Engineering for Industry*, 113:412–418, 1991.

[19] S. Moaveni. *Finite Element Analysis: Theory and Application with Ansys*. Prentice Hall PTR, Upper Saddle River, NJ, USA, 1999.

[20] M. Moll and L. Kavraki. Path planning for deformable linear objects. *IEEE Trans. Robotics*, 22(4):625–636, Aug. 2006.

[21] S. Patil and R. Alterovitz. Automated tissue retraction for robot-assisted surgical procedures. In *IEEE Int. Conf. Rob. and Aut.*, 2010.

[22] S. Rodriguez, J.-M. Lien, and N. M. Amato. Planning motion in completely deformable environments. In *IEEE Int. Conf. on Robotics and Automation*, pages 2466–2471, Orlando, FL, May 2006.

[23] M. Saha and P. Isto. Motion planning for robotic manipulation of deformable linear objects. In *IEEE Int. Conf. Rob. and Aut.*, pages 2478–2484, May 2006.

[24] G. Sutherland, P. McBeth, and D. Louw. Neuroarm: An mr compatible robot for microsurgery. In *Computer Assisted Radiology and Surgery*, volume 1256, pages 504–508, 2003.

[25] R. Taylor, P. Jensen, L. Whitcomb, A. Barnes, R. Kumar, D. Stoianovici, P. Gupta, Z. Wang, E. Dejuan, and L. Kavoussi. A Steady-Hand Robotic System for Microsurgical Augmentation. *Int. J. of Rob. Res.*, 18(12):1201–1210, 1999.

[26] R. Z. Tombropoulos, J. R. Adler, and J. Latombe. Carabeamer: A treatment planner for a robotic radiosurgical system with general kinematics. *Medical Image Analysis*, 3:3–3, 1999.

[27] M. Torabi, K. Hauser, R. Alterovitz, V. Duindam, and K. Goldberg. Guiding needle insertions using single-point tissue manipulation. In *IEEE Int. Conf. Rob. and Aut.*, May 2009.

[28] X. Yu, H. J. Chizeck, and B. Hannaford. Comparison of transient performance in the control of soft tissue grasping. In *IEEE/RSJ Int. Conf. Int. Rob. and Sys.*, San Diego, CA, October 2007.